Structure
Technical Advance

A Ferritin-Based Label for Cellular Electron Cryotomography

Qing Wang,[1] Christopher P. Mercogliano,[1] and Jan Löwe[1,*]
[1]MRC Laboratory of Molecular Biology, Hills Road, Cambridge CB2 0QH, UK
*Correspondence: jyl@mrc-lmb.cam.ac.uk
DOI 10.1016/j.str.2010.12.002

SUMMARY

Electron cryotomography provides nanometer resolution structural detail of thin biological specimens in a near-native state. Currently, its application is limited by the lack of a specific label for the identification of molecules. Our aim was to develop such a label, analogous to GFP used in fluorescence microscopy. Here, we demonstrate the use of *Escherichia coli* ferritin FtnA protein as a clonable label for electron cryotomography. Overproduced ferritin is visible in *E. coli* cells using cryotomography and fusing this label to a short membrane targeting sequence correctly directs the ferritin fusion to the membrane. Using two proteins with known subcellular localization patterns with this ferritin tag, also including GFP, we obtained essentially the same labeling patterns using electron cryotomography as compared with fluorescence light microscopy. Hence, the ferritin label localizes efficiently and faithfully and it will be a valuable tool for the unambiguous identification of molecules in cellular electron cryotomograms.

INTRODUCTION

Electron cryotomography of biological samples is one of the key frontiers in structural cell biology. It is currently the only method that allows pleomorphic structures, such as cells, organelles, and many macromolecular assemblies to be imaged at nanometer resolution in a near-native "frozen-hydrated" state. Thanks to technological advances and improved specimen preparation techniques, the pace of electron cryotomography research has rapidly increased in recent years (Robinson et al., 2007). For example, the application of cryotomography to study small prokaryotic cells has produced results of significant impact in the field of prokaryotic cell biology and delivered insights on their cytoskeletal elements and subcellular organization (Li and Jensen, 2009; Milne and Subramaniam, 2009).

The three-dimensional reconstructions ("tomograms") from tomography of thin specimens typically have a resolution of around 5 nm, at least ten times better than light microscopy, and contain unprecedented structural information. Yet, one of the biggest challenges in cellular tomography is to unambiguously identify structures of interest. Some structures can be identified by imaging cells in which the protein of interest has been overexpressed or depleted and one can then observe what appears or is affected (Komeili et al., 2006). Alternatively, correlation-based searching of tomograms with template structures has been used to locate relatively large complexes (Beck et al., 2009; Böhm et al., 2000). Although such methods have been used to locate the 26S proteasome and ribosomes in cellular tomograms at an acceptable fidelity, they are unlikely to be useful for the detection of smaller complexes. To mimic the success of labeling techniques (particularly fluorescent protein fusions) in light microscopy, attempts have been made to construct an electron-dense fusion tag for electron tomography. For example, the metal-binding protein metallothionein can be fused to a protein of interest to increase its contrast (Diestra et al., 2009; Mercogliano and DeRosier, 2007). However, the heavy metals required for labeling are toxic for cells, and it remains unclear if they can be transported into cells with the required efficiency. Another method is to use biarsenical compounds that can bind to a tetracysteine motif and be photoreacted within chemically fixed samples to provide contrast for localization (Gaietta et al., 2006). The advantage of this method is that it can be used in correlative microscopy where one can image the same specimen with both fluorescence light microscopy and electron microscopy (Giepmans, 2008). Unfortunately, this method requires a fixation step that tends to distort cellular structure and thus this approach moves away from the "near-native state" benefits of cryotomography.

When we started, we hypothesized that existing biological complexes could be engineered to function as labels for electron cryotomography. To fulfill the role of a tomography label, a complex must possess certain qualities: it must be suitable as a fusion partner for the gene of interest, it must have a suitable size and shape, it must be able to assemble efficiently in vivo and most importantly it must impart significantly higher contrast than the background environment within the tomogram. Here we show that ferritin fulfils these criteria. Ferritin particles have a small spherical protein shell assembled from the 19 kDa protein monomer with a central cavity that stores excess iron when cells grow in iron-rich conditions (Smith, 2004).

Here, we demonstrate that iron-loaded ferritin is visible in intact *E. coli* cells using electron cryotomography. We then used our ferritin-based label to study two *E. coli* proteins with different, known subcellular localization patterns. In both cases, our fusion label was clearly detected at the expected subcellular positions. These results show that ferritin-based labels are valuable tools for the localization and identification of molecules in cells with electron cryotomography.

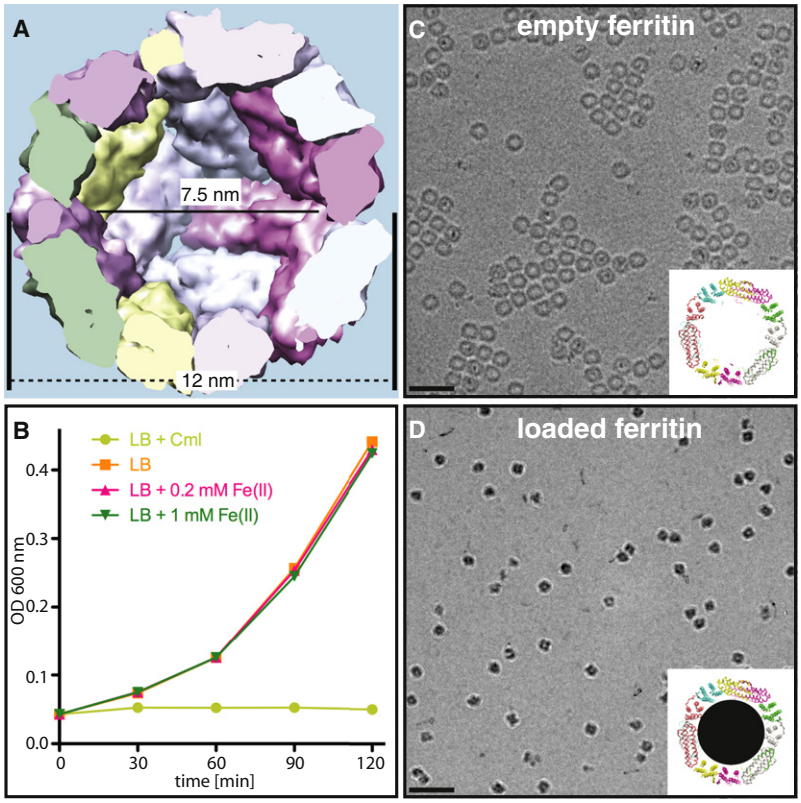

Figure 1. Assembly and Iron-Loading of Ferritin Overproduced in *E. coli*

(A) Surface representation of the crystal structure of *E. coli* FtnA protein (Stillman et al., 2001). Half of the ferritin shell is shown, exposing the inner cavity with a diameter of roughly 7.5 nm.

(B) Growth curves of *E. coli* cells grown in LB medium supplemented with 0, 0.2, or 1 mM of Fe(II), respectively. Medium with 10 μg/ml of Chloramphenicol is used as a control.

(C and D) Electron cryomicroscopy of empty and iron-loaded ferritin particles isolated from cells grown in LB medium or LB supplemented with 1 mM Fe(II), respectively.

Scale bars: 30 nm. See also Figure S1.

RESULTS

Iron-Loaded Ferritin Is Visible within Intact *E. coli* Cells

There are several types of ferritin in *E. coli*, including bacterial ferritin (FtnA), bacterioferritin (Bfr), and dodecameric ferritin (Dps). We chose to use the bacterial ferritin assembled from FtnA protein, since it has a suitable size of 12 nm in diameter and has been reported to be the major iron storage unit in *E. coli* (Smith, 2004). The FtnA ferritin (hereafter referred to as ferritin) shell is assembled from 24 identical 19.4 kDa FtnA monomers. Its central cavity is around 7.5 nm in diameter (Figure 1A) and becomes loaded with iron when cells grow under iron-rich conditions (Smith, 2004). In *E. coli*, the global iron-dependent regulator Fur protein represses the iron acquisition genes under iron sufficiency (Smith, 2004). As inactivating the *fur* gene has been suggested to increase free cellular iron concentration (Abdul-Tehrani et al., 1999) and thus facilitate loading of overexpressed ferritin, we constructed and used an *E. coli fur* knockout strain. Another advantage of using the *fur* knockout strain is that the upregulation of chromosomal ferritin genes by iron is abolished, therefore making it unnecessary to generate ferritin knockout strains. When these *E. coli* cells were grown in media supplemented with 0.2 or 1 mM Fe(II), we observed no obvious effect of the extra iron on cell growth, cell division or morphology (Figure 1B; see Figure S1 available online).

We first characterized the assembly and loading efficiency of ferritin overproduced in *E. coli* cells. Ferritin particles were overexpressed and purified from *E. coli* cells grown in rich media without extra Fe(II). Electron cryomicroscopy showed that these particles were mostly empty protein shells that had a diameter of roughly 12 nm, and a central cavity was clearly evident (Figure 1C). Next, FtnA was overexpressed in *E. coli Δfur* cells grown in rich media containing 1 mM Fe(II), and ferritin particles were purified from the cells. When these ferritin particles were examined using electron cryomicroscopy, we observed electron-dense dots between 4 and 7.5 nm in diameter (Figure 1D). Since iron produces higher contrast in electron micrographs than the light elements, it is clear that the dots observed in Figure 1D correspond to the iron cores of loaded ferritin particles. Their much higher contrast than protein makes it difficult to see ferritin shells at the same time. Similar result has been reported previously for iron-loaded horse spleen ferritin (Dubochet et al., 1988). After measuring 800 of the electron-dense dots, we determined that their average diameter was 7 nm, close to that reported for the central cavity of ferritin. A small amount of the electron-dense dots are much smaller than the rest (Figure 1D). These smaller dots are likely to be partially loaded or empty ferritin particles. They account for 8% of the total population analyzed, suggesting that up to 92% of the ferritin particles are loaded with iron (n = 800). It can be seen that the iron cores of ferritin are not spherical (Figure 1D) and the iron deposits on the inside seem to follow the shell's 432 point symmetry.

Having been able to assemble and load ferritin particles efficiently in vivo, we next explored whether or not they could be directly visualized inside cells by electron cryotomography. *E. coli* cells with a diameter of ~1 μm are too thick for high-resolution and high-contrast imaging by whole-cell tomography because the mean free path of 300 keV electrons in biological specimens is around 350 nm (Grimm et al., 1998). By growing a thinner *E. coli* strain (B/r H266) in minimal media, we were able to generate much thinner cells with a diameter of ~0.6 μm (Tureba and Woldringh, 1980). Such cells are more suitable for whole-cell tomography experiments. Figure 2A shows a longitudinal slice through the tomogram of a cell with ferritin overexpressed in the presence of 1 mM of Fe(II). Excitingly, high-contrast dots with a diameter of ~7 nm, similar to those observed in vitro for loaded ferritin particles, were clearly visible in these tomograms (Figures 2A, left, 2C, and 2D; Movie S1). We

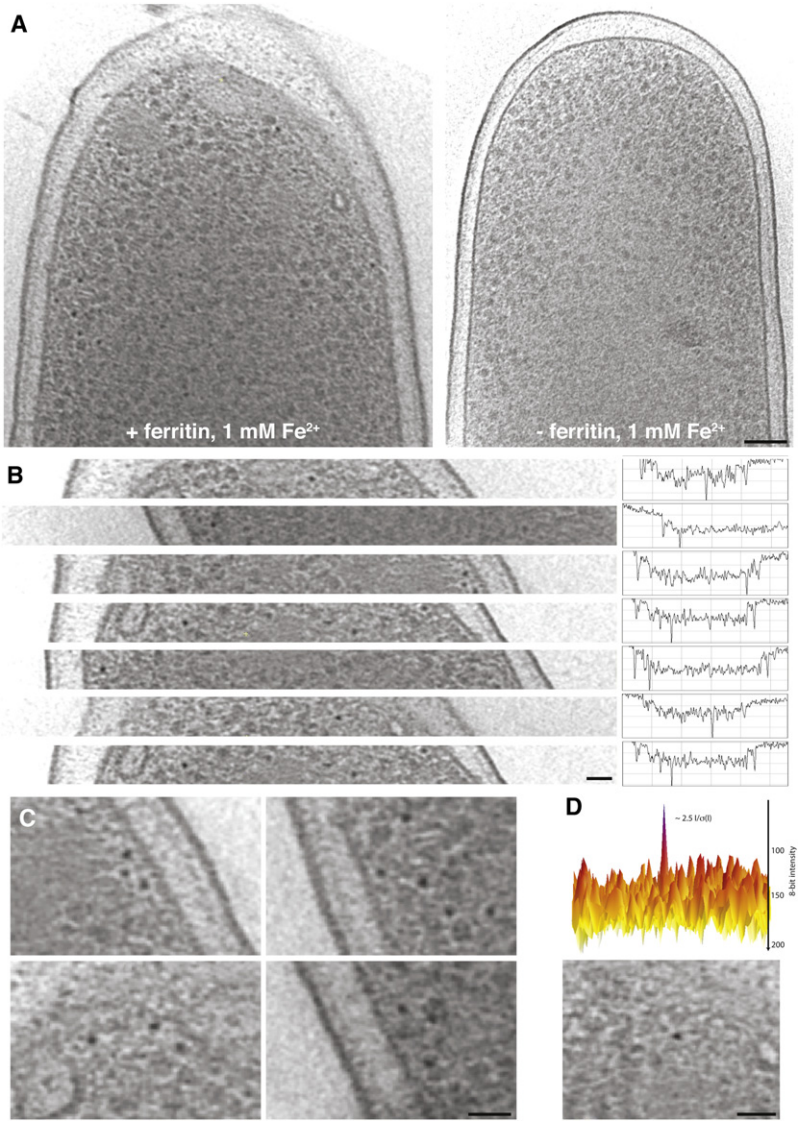

Figure 2. Direct Visualization of Ferritin Inside *E. coli* Cells by Electron Cryotomography

(A) Visual comparison of tomogram slices of cells grown in M9 media with 1 mM iron and with or without overproducing ferritin.

(B) Slices through tomograms of cells with ferritin overexpressed (left) and density profile along the slices (right), showing peaks at positions corresponding to location of putative ferritin dots.

(C) Higher magnification of regions in (A) containing multiple ferritin dots.

(D) 3D surface plot of a region in the tomogram slice with a peak corresponding to the ferritin dot near the center.

Scale bars: 100 nm for (A), and 50 nm for (B)–(D). See also Movie S1.

then looked at density profiles along the tomogram slices. Figure 2B shows well-resolved peaks of 2–3 sigma height at positions corresponding to electron-dense dots along the slice of the tomogram that most likely result from iron-filled ferritin. These electron-dense dots were not (or very rarely) seen in tomograms of cells overexpressing ferritin but grown in low-iron medium, or in cells not expressing ferritin grown in iron-rich medium (Figure 2A, right). Therefore, we reasoned that these high-contrast dots were the iron-cores of loaded ferritin particles, and that they could be visualized directly inside intact cells.

Tethering Ferritin to the Cytoplasmic Membrane of *E. coli*

To determine whether ferritin can be directed to specific subcellular regions, we fused the membrane targeting sequence (mts) from the *E. coli minD* gene followed by GFP to the N terminus of FtnA, giving rise to mts-GFP-FtnA, and investigated the in vivo localization pattern of this ferritin fusion, which we termed mts-ferritin (Figure 3A). Fluorescence light microscopy of cells expressing mts-ferritin showed that it localizes to the cell poles and also formed punctae close to the cytoplasmic membrane (Figure 3B). The assembly and iron-loading capabilities of these fusion proteins were assessed by comparing negatively stained and un-stained electron micrographs using mts-ferritin purified from cells grown in medium with 0.4 mM Fe(II). According to this, more than 60% of the mts-ferritin was iron-loaded (data not shown).

We next imaged cells expressing mts-ferritin with electron cryotomography. Longitudinal slices through tomograms of two such cells revealed that mts-ferritin localized to both the cytoplasmic membrane and to the periphery of membrane vesicles formed near the cell poles (Figures 3C and 3E; Movies S2 and S3). The membrane vesicles we observed are likely to be caused by the overexpression of mts-ferritin since we have observed on multiple occasions that overexpression of peripheral membrane proteins, especially those that oligomerize or polymerize, tends to generate membrane vesicles inside cells. The distance between the center of ferritin dots and cytoplasmic membrane was measured to be ~11 nm (see Figure S2). This value is very close to the estimated radius of mts-ferritin, suggesting the dots we observed in cells are iron cores of mts-ferritin particles. In the cell shown in Figure 3E, mts-ferritin particles all localized close to the cytoplasmic membrane. The relative positions of the mts-ferritin particles are better illustrated by the 3D segmentation (Figures 3D and 3F) because in print only one section can be shown easily. It is worth mentioning that the mts-ferritin tends to localize in small clusters, closely resembling the punctae observed with fluorescence light microscopy. In all tomograms we have taken (n = 12) (see also Figure S2), mts-ferritin always localized to the cytoplasmic membrane or polar membrane vesicles. Hence, we conclude that ferritin can be used as a fusion tag to locate specific regions inside cells.

Labeling the Chemosensory Machinery in *E. coli*

One of the bacterial protein complexes known to occupy a specified subcellular region is the *E. coli* chemosensory machinery

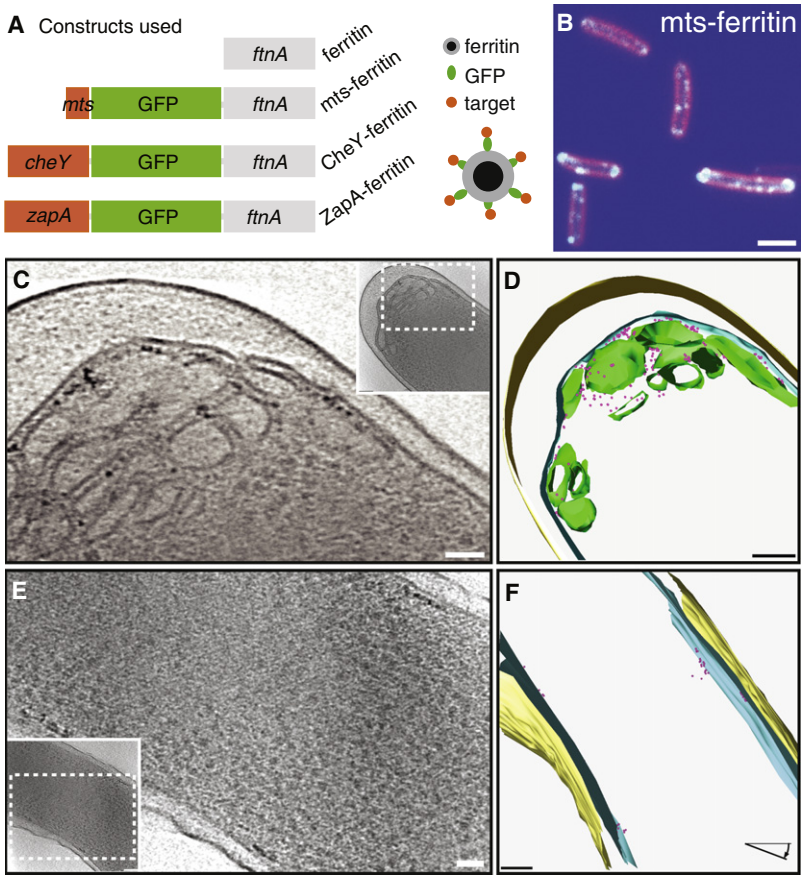

Figure 3. Ferritin Can Be Tethered to the Cytoplasmic Membrane with a Membrane Targeting Sequence (mts)

(A) Diagram showing all ferritin constructs used in this study, and a cartoon illustrating one ferritin fusion particle (only 6 out of 24 fusion partners are shown).

(B) Fluorescence microscopy image of cells expressing mts-GFP-FtnA (green) stained with FM4-64 (pink) for membrane.

(C) and (E) 10 nm slices through tomograms for cells expressing mts-ferritin. Insets show the same cells at a lower magnification.

(D) and (F) 3D segmentations of the inner membrane (cyan), outer membrane (yellow), membrane vesicles (green) and mts-ferritin (pink) in tomograms of the same cells in (C) and (E). Scale bar: 2 μm for (B), 50 nm for (C) and (E), and 100 nm for (D) and (F). See also Figure S2 and Movies S2 and S3.

(Maddock and Shapiro, 1993). The transmembrane chemoreceptors form clusters at the cell poles. Typically, the majority of the complexes localizes to a single pole under wild-type conditions. Other components of the chemosensory complex further associate with these chemoreceptors (Kentner and Sourjik, 2006). Due to their localization at the relatively thin cell pole region, chemoreceptors were among the first structures to be imaged by tomography of intact *E. coli* cells (Zhang et al., 2007). We were able to image both the chemoreceptor arrays and the associated histidine kinase CheA protein of the two-component signal transduction pathway, unlabelled (Figure 4C). Since the chemosensory machinery appears as a relatively stable structure and is easily recognizable in tomograms, it provided a good test case for our ferritin label. We chose to tag the response regulator CheY of the chemotaxis two-component system with the ferritin label. CheY is known to interact with CheA, and colocalizes with the chemoreceptors when overexpressed (Kentner and Sourjik, 2006). To this end, CheY followed by GFP was fused to the N terminus of FtnA, giving rise to CheY-GFP-FtnA. We term the ferritin assembled from CheY-GFP-FtnA protein CheY-ferritin (Figure 3A). Based on fluorescence light microscopy, this construct localized to one pole in each cell for more than 95% of cells observed (n = 100, Figure 4A). Hence, the GFP-FtnA moiety and the ferritin tagging did not substantially affect the correct localization of CheY-ferritin. Moreover, electron microscopy of purified ferritin particles from cells overexpressing CheY-ferritin showed that they were able to assemble and be loaded with iron at an efficiency of ~60% (data not shown).

Cells expressing CheY-ferritin were then imaged by electron cryotomography. Interestingly, CheY-ferritin formed a string of particles parallel to the cytoplasmic membrane at the cell pole (Figure 4D; Movie S4). The chemoreceptor arrays in these tomograms were not as obvious as those shown in Figure 4C, possibly because disproportionately high levels of CheY fusion protein may affect organization of chemosensory machineries as previously reported (Zhang et al., 2007). Nevertheless, they confirm that CheY-ferritin localized to the chemoreceptors. 3D segmentation for the tomogram in Figure 3D gives a clearer overview of the relative localization of CheY-ferritin and chemoreceptors. We could see that CheY-ferritin localizes close to the surface of the chemoreceptors, and covers nearly half of their surface area (Figure 4E). In the 12 tomograms of half-cells observed (see Figure S3), we either saw labeling of chemoreceptors with CheY-ferritin at the cell pole, or no chemoreceptors and no CheY-ferritin. Four of these tomograms were taken of each of the poles of a single cell, and we saw labeling of chemoreceptors by CheY-ferritin in only one pole for each pair as expected (see Figure S3).

It has been reported that chemoreceptors form additional lateral clusters in filamentous cells where cell division is blocked by the antibiotic cephalexin (Thiem et al., 2007). Indeed, fluorescence light microscopy showed that more than 80% of the cephalexin-treated cells (n = 100) contained lateral clusters of CheY-ferritin (Figure 4B). In tomograms of these cephalexin-treated cells, 60% contained lateral CheY-ferritin clusters (n = 10) (see Figure S4). A tomogram and 3D segmentation for a cell containing both polar and lateral chemoreceptor clusters labeled by CheY-ferritin is shown in Figures 4F and 4G. In summary, the labeling patterns by the CheY-ferritin tags are very similar to those from fluorescence light microscopy under all conditions we have tested. Thus, our CheY-ferritin label can tag the chemosensory machinery faithfully and efficiently.

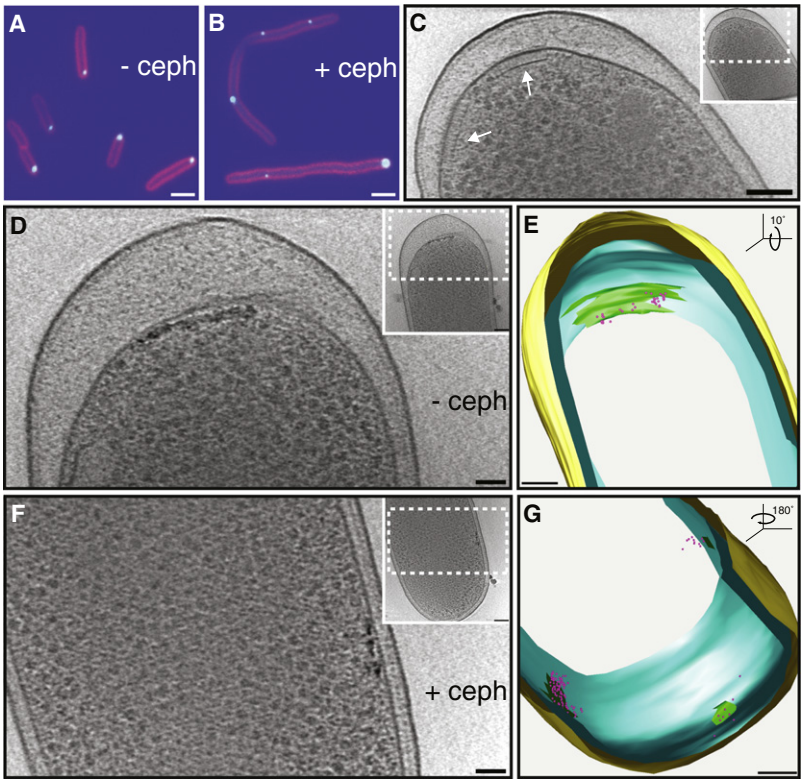

Figure 4. Ferritin Labeling the Chemosensory Machinery of *E. coli*

(A and B) Fluorescence microscopy images of cells expressing CheY-GFP-FtnA (green) stained with FM4-64 (pink) for membrane. Cells in (B) were treated with 10 μg/ml cephalexin for 2 hr.

(C) Slice (10 nm) through the tomogram of a cell with visible chemoreceptor arrays (white arrows) near the cell pole. Inset shows the same cell at a lower magnification.

(D) and (F) 10 nm slices through tomograms of cells expressing CheY-ferritin. The cell shown in (F) was treated with cephalexin as described for (B). Insets show the same cells at a lower magnification.

(E) and (G) 3D segmentations of the inner membrane (cyan), outer membrane (yellow), CheY-ferritin (pink), and putative chemoreceptor clusters (green) in tomograms of the same cells in (D) and (F), respectively.

Scale bar: 2 μm for (A) and (B), 50 nm for (D) and (F), and 100 nm for (E) and (G). See also Figures S3 and S4 and Movie S4.

Labeling the Septum of Dividing *E. coli*

We also attempted to label the cell division site, or septum, of *E. coli*. During bacterial cell division, the tubulin homolog FtsZ forms a ring-like structure at the septum, which acts as a scaffold for the assembly of a dozen of additional proteins involved in cell division (Goehring and Beckwith, 2005). One of the proteins known to associate with the FtsZ ring structure is ZapA (Gueiros-Filho and Losick, 2002). We chose to label the septum by tagging ZapA with ferritin, given that this protein has been shown to tolerate major genetic manipulations and has very little effect on cell division when overexpressed, in contrast to other components of the divisome (Goehring et al., 2005). We constructed a ZapA-GFP-FtnA fusion (designated ZapA-ferritin) by fusing ZapA followed by GFP to the N terminus of FtnA (Figure 3A), and characterized its localization pattern by fluorescence light microscopy. When ZapA-ferritin was expressed at low levels, it formed bands at the division site and sometimes also localized to cell poles (Figure 5A). In elongated cells, ZapA-ferritin also formed bands at one-quarter and three-quarter positions in addition to the patterns described above. When the fusion protein was expressed at higher levels, the cells became much longer, indicating a detrimental effect on cell division. In most of the elongated cells, ZapA-ferritin formed bands in the mid-cell regions where cell constriction had started (Figure 5B). Therefore, ZapA-ferritin was able to localize to the septum under both conditions. Based on electron microscopy of purified ZapA-ferritin, about 30% was loaded with iron (data not shown). It is currently unclear why the loading efficiency is low compared with the other constructs we investigated.

We next imaged cells expressing ZapA-ferritin with electron cryotomography. Tomograms were taken for the septum regions (n = 18) and cell poles (n = 4) (see Figure S5). ZapA-ferritin was observed in 66% of the septum tomograms. In tomograms for septum regions, more than 80% of ZapA-ferritin localized very close to the invaginating cytoplasmic membrane, whereas the remaining ZapA-ferritin fusion particles also assembled near the septum. Figures 5C–5E show slices through the tomograms of three cells and these demonstrate that ZapA-ferritin localized close to the invaginating cytoplasmic membrane (Figures 5C–5E; Movie S5). In the 3D segmentation of the tomogram for the septum region, ZapA-ferritin appeared to localize on the septal plane, and located close to the invaginating cytoplasmic membrane (Figures 5D and 5E), which is consistent with septal ring formation. In 50% of the tomograms taken for cell poles, we observed ZapA-ferritin near the cytoplasmic membrane region at the cell poles (data not shown). Hence, ZapA-ferritin generates a labeling pattern with satisfactory fidelity, even for a dynamic biological process such as cell division.

DISCUSSION

Ferritin as a Label for Cellular Tomography

We have shown that bacterial ferritin FtnA of *E. coli* assembles and loads efficiently when overexpressed in *E. coli* cells, and iron-loaded ferritin particles can be observed directly within intact cells by electron cryotomography (Figures 1 and 2). Although the dense cytoplasm of *E. coli* limits the resolution attainable and signal-to-noise ratio of cryotomograms, the electron-dense iron-core of ferritin can be recognized with about 2–3 sigma over background (Figure 2). In the future, it may be possible to use the 432 symmetric structure of the iron core to search for ferritin within tomograms using a template matching method. Also, it has not escaped our attention that the iron core of ferritin might lend itself to direct detection with electron

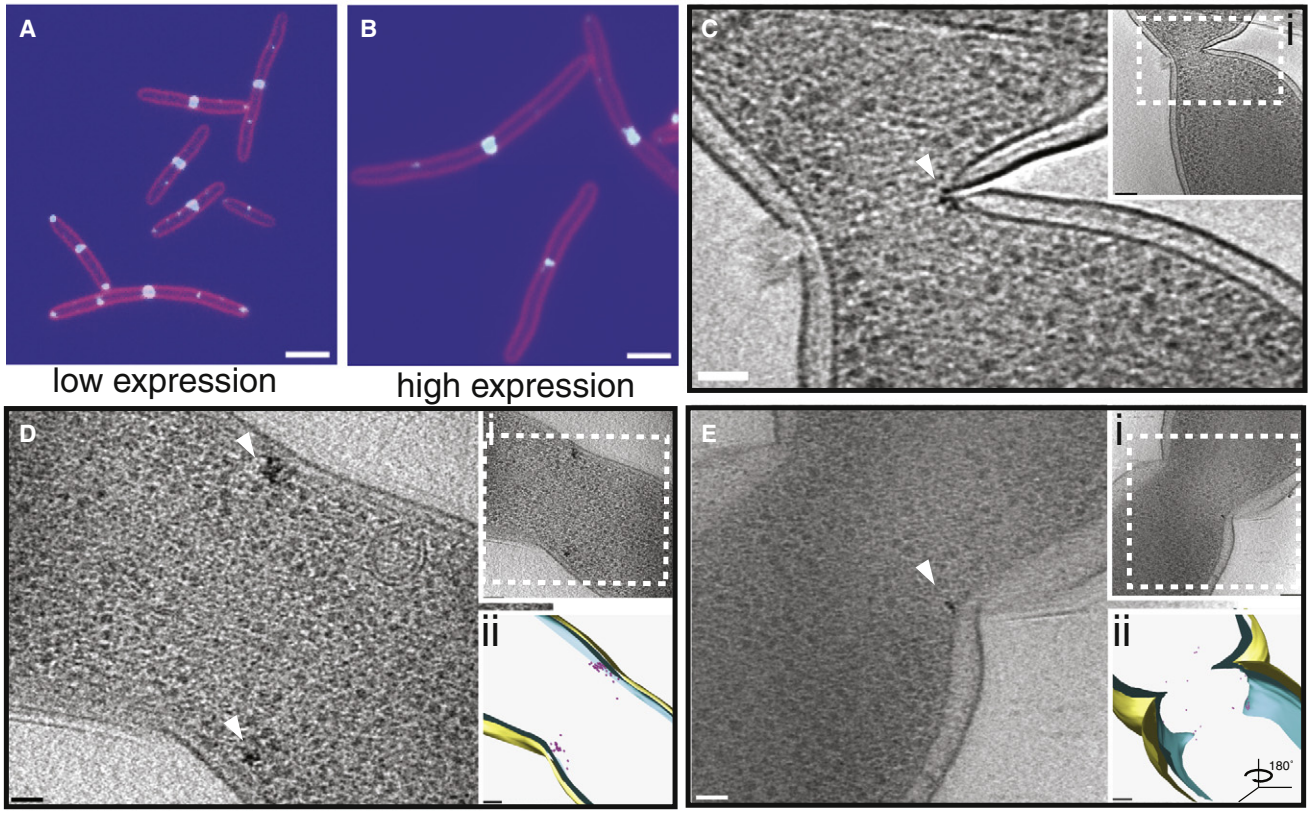

Figure 5. Ferritin Labeling the Septum of *E. coli* with ZapA

(A) and (B) Fluorescence microscopy images of cells expressing low and high levels of ZapA-GFP-FtnA (green) stained with FM4-64 (pink) for membrane.

(C–E) 10 nm slices through the tomograms of septum regions of cells expressing ZapA-ferritin (marked with white arrowheads). Insets (i) show the same cells at a lower magnification. Insets (ii) show the 3D segmentation of the inner membrane (cyan), outer membrane (yellow), and ZapA-ferritin (pink) in tomogram of the same cells.

Scale bars: 2 μm for (A) and (B), 50 nm for (C)–(E), and 100 nm for insets in (C)–(E). See also Figure S5 and Movie S5.

energy loss spectroscopy (EELS) imaging using an appropriately set energy filter.

The high efficiency of assembly and loading, suitable size, and the high contrast of the iron core make ferritin a promising label for identification of molecules in cellular tomograms. Importantly, when ferritin was fused to a membrane targeting sequence, the mts-ferritin fusion became attached to the cytoplasmic membrane or to membrane vesicles formed near cell poles (Figure 3). This suggests that ferritin fusions are able to diffuse inside cells and can potentially approach targeted cellular regions, or that the majority of the fusion protein is directed to the targeted subcellular region where assembly and iron-loading then occur.

Labeling Subcellular Structures with the Ferritin Tag

In order to assess the functionality of our ferritin labels, we tagged two protein complexes with known localization inside *E. coli* cells: the chemosensory machinery and the cell septum. In both cases, the fusion proteins used for ferritin tagging were assembled and loaded efficiently enough to ascertain localization patterns. Electron cryotomography data showed that the ferritin tag localized to the target of interest with high fidelity and efficiency, certainly in the case of the chemosensory machinery. Moreover, the localization patterns fitted closely to those from fluorescence light microscopy in both examples (Figures 4 and 5).

In a similar fashion to GFP labeling for fluorescence light microscopy, the fidelity and accuracy for localization of molecules with this ferritin tag are expected to be higher for more stable complexes and structures with a higher local concentration in cells. Consistently, the labeling efficiency was the highest for chemoreceptors, and almost every cell randomly selected for tomography had the expected localization pattern.

Comparison with Other Labeling Methods

Compared with much more developed labeling techniques employed in fluorescence light microscopy, we have currently no universally working method for the specific labeling of molecules in cryotomography of whole cells. This is mainly due to the contradictory requirements for a functioning electron microscopy label regarding size and contrast. For example, the nanostructure used as a label has to be large enough to be recognizable in electron cryotomograms, and yet be small enough to be able to assemble and/or get transported into cells at a high efficiency, while not perturbing the local cellular environment significantly.

So far, successful application of the metallothionein label and tetracysteine-ReAsH tagging method has been very limited, due to problems including toxicity of heavy metals used with the metallothionein label, and the sample fixation procedure and large size of the deposits in tetracysteine-ReAsH tagging (Diestra et al., 2009; Gaietta et al., 2006). There are obviously also limits of our ferritin-based labels. First, it is a relatively large structure of >12 nm diameter. Fusing such a structure may lead to mislocalization of the target protein, as is often seen even with the much smaller GFP fusion tag used in light microscopy (Werner et al., 2009). Therefore, careful controls must be undertaken to ensure correct localization pattern of the fusion particle and to avoid artifacts when using ferritin-based labels. This is why we used a double label approach that allows visualization with GFP in living cells using fluorescence light microscopy. Second, the multivalent nature of the ferritin particle might affect the structures to be labeled. For example, clustering of mts-ferritin particles and also of ferritin-bound membrane vesicles was observed when labeling with mts-ferritin, and this is most likely due to the presence of 24 fusion partners in each ferritin particle as illustrated in Figure 3. Third, the molecules used to direct ferritin fusions to the target are often overexpressed at higher levels than they would be under physiological conditions. Nevertheless, we believe it will be possible to overcome the stated problems in the future with better design of the ferritin label. For example, it may be possible to fuse two or more ferritin subunits together using a flexible linker. Combining this idea with the method to coexpress tagged and untagged ferritin proteins at a suitable ratio (for example, 1:1), it might be possible to reduce the target binding sites of ferritin particles by a factor of four to six.

The advantages of our ferritin label include its high imaging contrast and low toxicity for the biological system. The high-contrast iron-core of ferritin is recognized easily above background, and almost as easily as colloidal gold particles in immune-gold labeling of resin-embedded thin sections. Yet, it is advantageous over immunogold labeling since ferritin-based labels reveals three-dimensional information, in contrast to colloidal gold that is restricted to section surfaces (Schwarz and Humbel, 1989). Moreover, the procedure for ferritin labeling is quick and simple, and the specimen is preserved in a near-native state at cryotemperatures throughout the procedure. In addition, inclusion of a fluorescent protein moiety in the ferritin tag provides the possibility of using the tagging system in correlated electron and light microscopy (Sartori et al., 2007). This will greatly simplify the steps of searching for regions of interest and will undoubtedly be valuable when using the tag to study more dynamic or unknown cellular processes.

EXPERIMENTAL PROCEDURES

Plasmids and Strains

All plasmids used in this study are derivatives of pBAD24 (Guzman et al., 1995). In brief, wild-type FtnA ferritin was expressed using plasmid pQW146, constructed by cloning the *ftnA* gene of *E. coli* into pBAD24. Plasmid pQW156 encodes FtnA with an N-terminal 6xhis tag. GFP was cloned into pQW146 using the In-Fusion PCR Cloning kit (Clontech, Mountain View, CA), yielding plasmid pQW150 encoding the fusion protein GFP-FtnA. The three plasmids for expression of the ferritin tags were constructed by PCR cloning the C-terminal 16 amino acids encoding the amphipathic helix of *minD* (residues 255–270, GenBank: 945741) (Hu and Lutkenhaus, 2003), the *cheY* gene (GenBank: 946393), and the *zapA* gene of *E. coli* (GenBank: 947404) to the N terminus of GFP in pQW150, yielding plasmids pQW154, pQW152, pQW153, respectively. The *fur* knockout mutation from *E. coli* strain EM1256 was introduced into the thin *E. coli* mutant strain B/r H266 by P1-transduction (Masse and Gottesman, 2002). The resulting strain was used for all experiments throughout the study.

Media and Growth Conditions

LB media was used in all experiments for overexpressing ferritin and ferritin fusions to be isolated for in vitro assays. Cells carrying the expression plasmid were grown at 37°C and induced with 0.2% arabinose for 3 hr. For growth in iron-rich conditions, $FeSO_4$ was added into the growth medium to a final concentration of 1 mM at the same time as arabinose. Cells for electron cryotomography experiments were grown in M9 minimal media (to make them even thinner) supplemented with 0.4% glycerol at 30°C. Protein expression was induced with 0.06–0.1% arabinose for 2–3 hr in the presence of 0.2–1 mM $FeSO_4$. Antibiotics ampicillin and kanamycin were used at concentrations of 100 and 30 μg/ml, respectively.

Ferritin Isolation

Ferritin and ferritin fusions were purified by size-exclusion chromatography of the clarified cell lysate using Sepharose 6B resin and PBS, except that his-tagged ferritin was first purified using a His-Trap column (GE Healthcare). Ferritin particles were highly enriched in the early eluted fractions, which were pooled for further analysis.

Electron Microscopy

Samples of isolated ferritin were visualized with a Tecnai 12 electron microscope operating at 120 kV. The specimens were either briefly stained with 0.5% uranyl acetate for 10 s, or unstained, and electron micrographs were recorded at a pixel size of 0.72 nm. Electron cryomicroscopy of purified ferritin was performed with an FEI Tecnai G2 Polara microscope operating at 80 kV and electron micrographs were recorded with a (pre-GIF) 2 × 2 k Gatan Ultrascan CCD camera binned to 1 × 1 k (Gatan, Pleasanton) at a pixel size of 0.46 nm, and a defocus of −1.5 μm.

Cells for electron cryotomography were mixed with 10 nm gold-conjugated protein A, and plunge-frozen on a glow-discharged holey carbon grid (Quantifoil, Cu/Rh 300 mesh, R3.5/1) into liquid ethane using an FEI Vitrobot (FEI Company, Eindhoven, The Netherlands). The grids were transferred to and stored in liquid nitrogen.

Electron cryotomography imaging was performed at 300 kV on an FEI Tecnai G2 Polara microscope equipped with a Gatan energy filter (filter bandpass 20 eV) and a (post-GIF) 4 × 4 k Gatan Ultrascan CCD camera binned to 2 × 2 k (Gatan, Pleasanton, CA). Tilt series were collected around a single axis at a 1° increment between ±50° at a pixel size of 0.58 nm using SerialEM software (Mastronarde, 2005). The defocus was set at −12 μm and the cumulative dose was between 160 and 200 e/Å^2.

Fluorescence Microscopy

Cells used for fluorescence light microscopy were grown at the same conditions as those used for electron cryotomography. Cells were washed with PBS once, membrane stained with 10 μg/ml FM4-64 for 3 minutes, and were then applied to an agarose pad on a microscope slide. A Nikon Eclipse E800 microscope with Plan Apo 100×/1.40 oil DIC objective and a Photometrics Coolsnap HQ2 camera was used for imaging.

Image Processing

Tomographic reconstructions were calculated using both the IMOD tomography package and the Priism software using the SIRT algorithm (Chen et al., 1992; Kremer et al., 1996). 3D segmentation of tomograms was carried out using the IMOD software. Images from the GFP channel and FM4-64 channel of fluorescence light microscopy were processed and merged using Adobe Photoshop CS3 (Adobe Systems Incorporated).

SUPPLEMENTAL INFORMATION

Supplemental Information includes five figures and five movies and can be found with this article online at doi:10.1016/j.str.2010.12.002.

ACKNOWLEDGMENTS

We thank Shaoxia Chen (MRC-LMB, Cambridge, UK) and Sergej Masich (Karolinska Institute, Stockholm, Sweden) for advice on EM techniques, Benoit Zuber (MRC-LMB, Cambridge, UK) for help with data processing and members of the Löwe group for advice and discussion. Q.W. is supported by a Dorothy Hodgkin Award from Cambridge University Overseas Trust.

Received: November 9, 2010
Revised: December 6, 2010
Accepted: December 10, 2010
Published: February 8, 2011

REFERENCES

Abdul-Tehrani, H., Hudson, A.J., Chang, Y.S., Timms, A.R., Hawkins, C., Williams, J.M., Harrison, P.M., Guest, J.R., and Andrews, S.C. (1999). Ferritin mutants of *Escherichia coli* are iron deficient and growth impaired, and *fur* mutants are iron deficient. J. Bacteriol. *181*, 1425–1428.

Beck, M., Malmstrom, J.A., Lange, V., Schmidt, A., Deutsch, E.W., and Aebersold, R. (2009). Visual proteomics of the human pathogen *Leptospira interrogans*. Nat. Methods *6*, 817–823.

Böhm, J., Frangakis, A.S., Hegerl, R., Nickell, S., Typke, D., and Baumeister, W. (2000). Toward detecting and identifying macromolecules in a cellular context: template matching applied to electron tomograms. Proc. Natl. Acad. Sci. USA *97*, 14245–14250.

Chen, H., Clyborne, W., Sedat, J.W., and Agard, D. (1992). PRIIMS: an integrated system for display and analysis of three-dimensional microscope images. Proc. SPIE *1660*, 784–790.

Diestra, E., Fontana, J., Guichard, P., Marco, S., and Risco, C. (2009). Visualization of proteins in intact cells with a clonable tag for electron microscopy. J. Struct. Biol. *165*, 157–168.

Dubochet, J., Adrian, M., Chang, J.J., Homo, J., Lepault, J., McDowall, A.W., and Schultz, P. (1988). Cryo-electron microscopy of vitrified specimens. Q. Rev. Biophys. *2*, 129–228.

Gaietta, G.M., Giepmans, B.N., Deerinck, T.J., Smith, W.B., Ngan, L., Llopis, J., Adams, S.R., Tsien, R.Y., and Ellisman, M.H. (2006). Golgi twins in late mitosis revealed by genetically encoded tags for live cell imaging and correlated electron microscopy. Proc. Natl. Acad. Sci. USA *103*, 17777–17782.

Giepmans, B.N. (2008). Bridging fluorescence microscopy and electron microscopy. Histochem. Cell Biol. *130*, 211–217.

Goehring, N.W., and Beckwith, J. (2005). Diverse paths to the midcell: assembly of the bacterial cell division machinery. Curr. Biol. *15*, R514–R526.

Goehring, N.W., Gueiros-Filho, F., and Beckwith, J. (2005). Premature targeting of a cell division protein to midcell allow dissection of divisome assembly in *Escherichia coli*. Genes Dev. *19*, 127–137.

Grimm, R., Singh, H., Rachel, R., Typke, D., Zillig, W., and Baumeister, W. (1998). Electron tomography of ice-embedded prokaryotic cells. Biophys. J. *74*, 1031–1042.

Gueiros-Filho, F.J., and Losick, R. (2002). A widely conserved bacterial cell division protein that promotes assembly of the tubulin-like protein FtsZ. Genes Dev. *16*, 2544–2556.

Guzman, L.M., Belin, D., Carson, M.J., and Beckwith, J. (1995). Tight regulation, modulation, and high-level expression by vectors containing the arabinose pBAD promoter. J. Bacteriol. *177*, 4121–4130.

Hu, Z., and Lutkenhaus, J. (2003). A conserved sequence at the C-terminus of MinD is required for binding to the membrane and targeting MinC to the septum. Mol. Microbiol. *47*, 345–355.

Schwarz, H., and Humbel, B.M. (1989). Influence of fixatives and embedding media on immunolabelling of freeze-substituted cells. Scanning Microsc. Suppl. *3*, 57–63.

Kentner, D., and Sourjik, V. (2006). Spatial organization of the bacterial chemotaxis system. Curr. Opin. Microbiol. *9*, 619–624.

Komeili, A., Li, Z., Newman, D.K., and Jensen, G.J. (2006). Magnetosomes are cell membrane invaginations organized by the actin-like protein MamK. Science *5758*, 242–245.

Kremer, J.R., Mastronarde, D.N., and McIntosh, J.R. (1996). Computer visualization of three-dimensional image data using IMOD. J. Struct. Biol. *116*, 71–76.

Li, Z., and Jensen, G.J. (2009). Electron cryotomography: a new view into microbial ultrastructure. Curr. Opin. Microbiol. *12*, 333–340.

Maddock, J.R., and Shapiro, L. (1993). Polar location of the chemoreceptor complex in the *Escherichia coli* cell. Science *259*, 1717–1723.

Masse, E., and Gottesman, S. (2002). A small RNA regulates the expression of genes involved in iron metabolism in *Escherichia coli*. Proc. Natl. Acad. Sci. USA *99*, 4620–4625.

Mastronarde, D.N. (2005). Automated electron microscope tomography using robust prediction of specimen movements. J. Struct. Biol. *152*, 36–51.

Mercogliano, C.P., and DeRosier, D.J. (2007). Concatenated metallothionein as a clonable gold label for electron microscopy. J. Struct. Biol. *160*, 70–82.

Milne, J.L., and Subramaniam, S. (2009). Cryo-electron tomography of bacteria: progress, challenges and future prospects. Nat. Rev. Microbiol. *7*, 666–675.

Robinson, C.V., Sali, A., and Baumeister, W. (2007). The molecular sociology of the cell. Nature *450*, 973–982.

Sartori, A., Gatz, R., Beck, F., Rigort, A., Baumeister, W., and Plitzko, J.M. (2007). Correlative microscopy: Bridging the gap between fluorescence light microscopy and cryo-electron tomography. J. Struct. Biol. *160*, 135–145.

Smith, J.L. (2004). The physiological role of ferritin-like compounds in bacteria. Crit. Rev. Microbiol. *30*, 173–185.

Stillman, T.J., Hempstead, P.D., Artymiuk, P.J., Andrews, S.C., Hudson, A.J., Treffry, A., Guest, J.R., and Harrison, P.M. (2001). The high-resolution X-ray crystallographic structure of the ferritin (EcFtnA) of *Escherichia coli*. J. Mol. Biol. *307*, 587–603.

Thiem, S., Kentner, D., and Sourjik, V. (2007). Positioning of chemosensory clusters in *E. coli* and its relation to cell division. EMBO J. *26*, 1615–1623.

Tureba, F.J., and Woldringh, C.L. (1980). Changes in cell diameter during the division cycle of *Escherichia coli*. J. Bacteriol. *142*, 869–878.

Werner, J.N., Chen, E.Y., Guberman, J.M., Zippilli, A.R., Irgon, J.J., and Gitai, Z. (2009). Quantitative genome-wide analysis of protein localisation in an asymmetric bacterium. Proc. Natl. Acad. Sci. USA *106*, 7858–7863.

Zhang, P., Khursigara, C.M., Hartnell, L.M., and Subramaniam, S. (2007). Direct visualization of *Escherichia coli* chemotaxis receptor arrays using cryo-electron microscopy. Proc. Natl. Acad. Sci. USA *104*, 3777–3781.

